102
640
THS

THESIS

This is to certify that the

thesis entitled
A STUDY OF CYCLIC STRESS AND
STRAIN CONCENTRATION FACTORS
AT NOTCH ROOTS THROUTHOUT
FATIGUE LIFE

presented by

Charles H. Bofferding III

has been accepted towards fulfillment
of the requirements for

Masters degree in Mechanics

John F. Martin
Major professor

Date 5/14/80

O-7639

OVERDUE FINES:
25¢ per day per item

RETURNING LIBRARY MATERIALS:
Place in book return to remo
charge from circulation reco

A STUDY OF CYCLIC STRESS AND STRAIN CONCENTRATION FACTORS AT NOTCH ROOTS THROUGHOUT FATIGUE LIFE

By

Charles H. Bofferding III

A THESIS

Submitted to
Michigan State University
in partial fulfillment of the requirements
for the degree of

MASTER OF SCIENCE

Department of Metallurgy, Mechanics and Materials Science

1980

ABSTRACT

A STUDY OF CYCLIC STRESS AND STRAIN CONCENTRATION FACTORS AT NOTCH ROOTS THROUGHOUT FATIGUE LIFE

By

Charles H. Bofferding III

Notch root stress and strain concentration factors, as related by Nueber's rule, are examined for various materials and notch geometries throughout fatigue life. Plates with circular and elliptic notches are cycled under constant amplitude load control (nominally elastic, completely reversed) in a hydraulic closed-loop fatigue system. Long and short life tests are run for each material and notch geometry. Strain at the notch root is recorded with the Interferrometric Strain Gage. The notch root strain is reproduced in a smooth sample, cycled under strain control, to produce local stress-strain hysterisis loops. These data are used to compute K_f.

ACKNOWLEDGEMENTS

The work for this thesis was funded by the National Science Foundation.

I would like to thank Lisa Adrian, Melvin Cartwright, Greg Hoshal and Tom Mase for their many hours of data reduction and drawing. Also special thanks goes to Dr. John Martin who gave me the opportunity, freedom and inspiration to accomplish this work.

TABLE OF CONTENTS

	Page
LIST OF TABLES	iv
LIST OF FIGURES	v
LIST OF SYMBOLS	vii
Chapter	
1. INTRODUCTION	1
2. THE INTERFEROMETRIC STRAIN GAGE	4
2.1 Fundamentals of the I.S.G.	4
2.2 Calibration of the I.S.G.	15
2.2.1 Strain to Fringe Shift	15
2.2.2 Fringe Shift to Voltage	15
2.2.3 Strain to Voltage	17
2.2.4 Calibration Test	17
2.2.5 Resolution	18
3. SAMPLES AND MATERIALS	20
4. EXPERIMENTAL METHODS	25
5. EXPERIMENTAL RESULTS	29
6. SUMMARY AND CONCLUSIONS	43
LIST OF REFERENCES	46

LIST OF TABLES

Table		Page
1	Material properties.	24
2	Test data.	30

LIST OF FIGURES

Figure		Page
1	Interferometric strain gage.	5
2	Indentations on sample.	6
3	Fringe generation principles.	7
4	Interference pattern.	8
5	I.S.G. schematic.	10
6	Electric analog to fringe pattern.	12
7	S_1 and S_2 for current mirror position 185.	13
8	Determination of maximum and minimum spacing.	14
9	I.S.G. vs. clip gage.	19
10	Computer printout of maximum and minimum.	19
11	Sample geometry.	21
12	Notch geometry.	22
13	Photograph of samples.	22
14	Indentations for 2024 elliptic sample before and after testing.	23
15	Output of cracked samples.	27
16	Test set up.	28
17	K_ε, K_σ, and K_f versus life for 1018 mild steel circular notches.	31
18	K_ε, K_σ, and K_f versus life for 1018 mild steel elliptical notches.	32
19	K_ε, K_σ, and K_f versus life for 2024 aluminum circular notches.	33

Figure		Page
20	K_ε, K_σ, and K_f versus life for 2024 aluminum elliptical notches.	34
21	K_ε, K_σ, and K_f versus life for 7475 aluminum circular notches.	35
22	K_ε, K_σ, and K_f versus life for 7475 aluminum elliptical notches.	36
23	K_f versus life for 1018 mild steel circular notches.	37
24	K_f versus life for 1018 mild steel elliptical notches.	38
25	K_f versus life for 2024 aluminum circular notches.	39
26	K_f versus life for 2024 aluminum elliptical notches.	40
27	K_f versus life for 7475 aluminum circular notches.	41
28	K_f versus life for 7475 aluminum elliptical notches.	42

31 K_1, K_2, and K_3 versus life for 7075 aluminum ... 35
circular notches.

32 K_1, K_2, and K_3 versus life for 7075 aluminum ... 36
elliptical notches.

LIST OF SYMBOLS

S^*: Nominal stress equals load divided by gross cross sectional area.

σ^*: Local or notch root stress.

e^*: Nominal normal strain.

ε^*: Local or notch root normal strain.

K_t: Theoretical stress concentration factor.

K_σ: Stress concentration factor $(\frac{\Delta\sigma}{\Delta S})$.

K_ε: Strain concentration factor $(\frac{\Delta\varepsilon}{\Delta e})$.

K_f: $[K_\sigma\ K_\varepsilon]^{\frac{1}{2}}$

E: Young's Modulus

*For fatigue these symbols are preceeded by Δ and are taken as ranges associated with one cycle.

138. OF BINDERS

CHAPTER 1

INTRODUCTION

Neuber's original equation (1)* equated the geometric mean of the notch stress and strain concentration factors to the theoretical stress concentration factor for a specific geometry and loading scheme, namely a V notch loaded in shear. Others have applied the relationship to various notch configurations usually under axial load to find good results in both elastic testing and, when proper limits are imposed on notch plasticity, plastic testing (2).

In the attempts to apply Neuber's rule to fatigue the stress and strain values of the monotonic relationship (S, σ, e, ε) are replaced with the stress and strain ranges of fatigue loading (ΔS, $\Delta\sigma$, Δe, Δe). In practice $[K_\sigma\ K_\varepsilon]^{\frac{1}{2}}$ equals a constant K_f which is less than K_t and Neuber's rule is written as:

$$K_f = [K_\sigma\ K_\varepsilon]^{\frac{1}{2}} = \left(\frac{\Delta\sigma}{\Delta S}\ \frac{\Delta\varepsilon}{\Delta e}\right)^{\frac{1}{2}}$$

Rearranging and multiplying both sides by E

$$K_f^{\,2}\ (\Delta S\ \Delta e\ E) = (\Delta\sigma\ \Delta\varepsilon\ E) \qquad [1]@$$

---

*Numbers in parenthesis refer to references listed in the reference table.
@Numbers in brackets refer to equations.

CHAPTER I

This equation shows that a function of changes in nominal stress and strain need only be multiplied by a constant concentration factor to obtain the value of the same function of changes in local stress and strain at the notch root.

Equation [1] reduces to the following form if the nominal stress and strain are limited to the elastic region (i.e., $\Delta eE = \Delta S$)

$$K_f \Delta S = (\Delta\sigma \Delta\varepsilon E)^{\frac{1}{2}} \quad [2]$$

The case where ΔS and Δe are elastic and $\Delta\sigma$ and $\Delta\varepsilon$ are inelastic covers many problems of engineering interest. At even lower values of S, the notch root remains essentially elastic and Equation 2 reduces to:

$$K_f \Delta S = \Delta\sigma \quad [3]$$

Equations [1] to [3] were derived by Topper et al. (3). They describe the relationship between nominal stress-strain behavior and local stress-strain behavior for the notch root. Equation [1] applies for all values of nominal stress, Equation [2] for values less than the yield stress, and Equation [3] for values less than the yield stress divided by K_f (i.e., elastic local stress). Also it is well known that the difference between K_t and K_f is greatest for sharp notches (15). It is recognized that these equations do not account for the complexity of mean stress and its relaxation nor variations in the stress and strain concentration factors due to cyclic material properties. However, Wetzel suggests the stress and strain ranges of smooth samples quickly converge to steady state values (11) and Blatherwick and Olson (7) and Crews and Hardrath (4) have shown that the notch root strain range also quickly stabilizes. Crews and Hardrath (4) assumed that the notch stress could be found by reproducing

Equation (3) reduces to the following form if the nominal stress

the notch strain in smooth samples. The stabilized local stress was then used to predict fatigue life of the notched sample with good results for nominally plastic ranges. Leis et al (17) extended this to nominally plastic ranges and examined K_ε and K_σ at the root to determine K_f. K_f was found to vary with life and strain ranges but tended to K_t with life. Using equations [1], [2], and [3] others have equated the stress-strain state at a notch to that of smooth sample and by applying cummulative damage methods have predicted notch fatigue life from smooth sample data (3, 7, 11, 13, 14, 15). (Note, this did not require subjecting smooth samples to notch root strains, only determining the notch stress-strain state with eq. [1], [2], or [3] and then using smooth sample fatigue-life data to predict failure).

Wetzel (11) examined these results (3, 4, 7, 13, 14, 15) to find that equations [1] to [3] accurately relate nominal and local stress-strain response even in non-linear applications and when used in conjunction with smooth sample data for 0-max loading yield good fatigue life predictions.

Both Crews and Leis et al. reported measurement problems associated with strain gages at the notch root. The purpose of this study is to overcome these problems in strain measurement and examine K_ε, K_σ, and K_f throughout fatigue life. This is done by measuring the notch root strain with the Interferometric Strain Gage (I.S.G.). The I.S.G. is a noncontacting laser based strain measuring system developed by Dr. William Sharpe and is fully described in this report.

CHAPTER 2

THE INTERFEROMETRIC STRAIN GAGE

2.1 Fundamentals of the I.S.G.

The Interferometric Strain Gage (20-23) is a noncontacting Laser based strain measuring system capable of measuring strain over a very small gage length (50-100 microns). Figure 1 shows the I.S.G.

The I.S.G. measures strain by monitoring the movement of interference fringes. The fringes are generated by interferring defraction patterns from two pyramidal indentations placed on a sample with a Vicker's hardness tester. The indentations generally measure 25 microns on a side and the center-to-center spacing between them is 100 microns. A picture of an indentation set is given in Figure 2. Figure 3 shows the principles involved in fringe generation. Incident monocromatic coherent laser light is reflected by the indentations. Each indentation creates a defraction pattern on both sides of the laser. On each side the defraction patterns interfer to create interferrence fringes. Any two interferring rays are out of phase by d $\sin\alpha$ where α is the angle between the incident laser and the interferring rays. Whenever:

$$d \sin\alpha = n\lambda \quad (n=0, \pm1, \pm2, \ldots) \qquad [4]$$

where: λ = wavelength of the laser light

the rays are in phase interferring constructively causing bright spots, Figure 4.

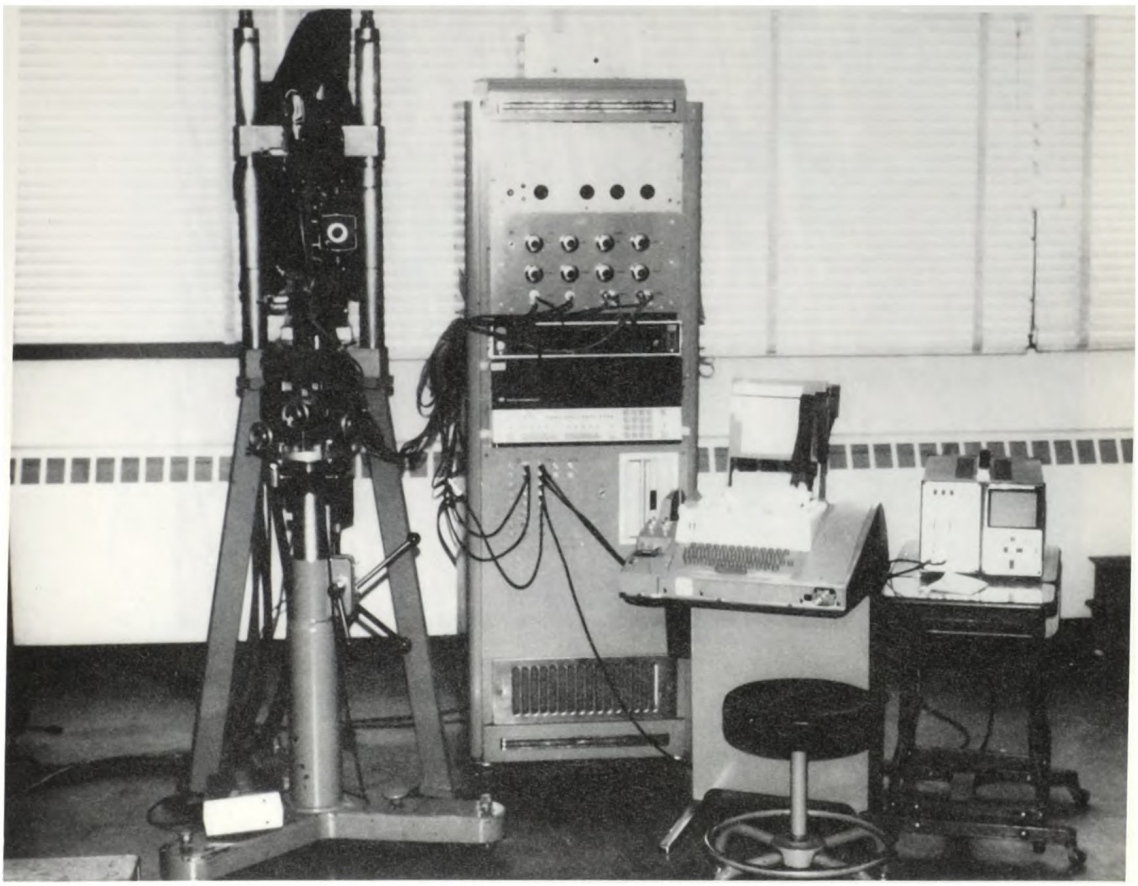

Figure 1 Interferometric Strain Gage

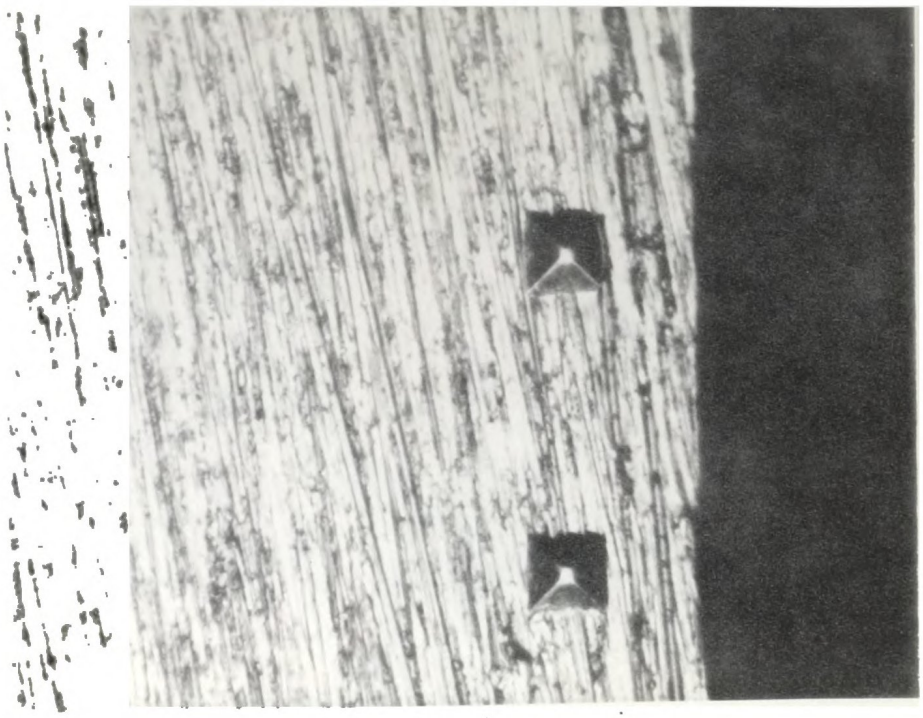

Figure 2 Indentations on Sample

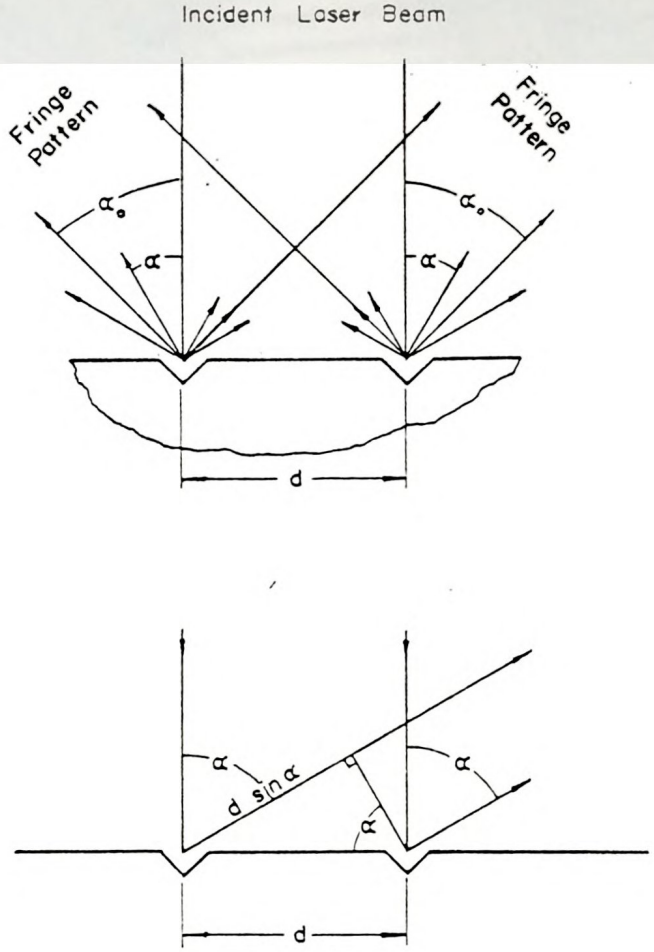

Figure 3 Fringe Generation Principles

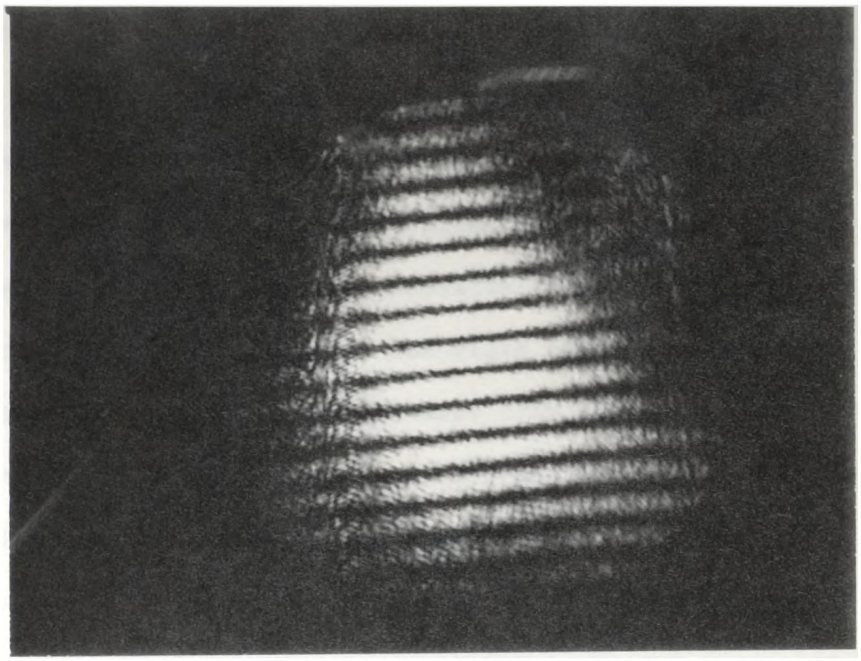

Figure 4 Interference Pattern

If the interference patterns are viewed from a stationary observation point defined by α_o any movement of the indentations is seen as a fringe shift past this point. For any one fringe in the patter d sinα in Equation [4] is a constant determined by a specific value of n. A tensile strain (increasing d) implies fringe movement toward the laser (decreasing α). Likewise a compressive strain will shift the fringes away from the incident laser. For rigid body motion one pattern will move toward the laser, the other away from it. If fringe movement toward the laser is measured as positive and movement away negative; averaging the fringe shift over the two channels cancels out rigid body motion.

Indentation and fringe movement for a channel are related by:

$$\delta d = \frac{\lambda}{\sin\alpha_o} \delta m$$

where: δm is the number or fraction of fringes passing the observation point

The two channel average is

$$\delta d = \frac{\lambda}{\sin\alpha_o} \left(\frac{\delta m_1 + \delta m_2}{2}\right)$$

A schematic of the I.S.G. is shown in Figure 5. It has two channels. Each monitors the movement of one interference pattern. The movement from both channels is averaged to cancel out rigid body motion as discribed.

For a given channel a servo mirror located at the stationary observation point reflects the interferrence pattern onto a slotted plate covering the PMT. This allows only a portion of the fringe pattern to be sensed by the PMT. By rotating the mirror the fringe pattern is

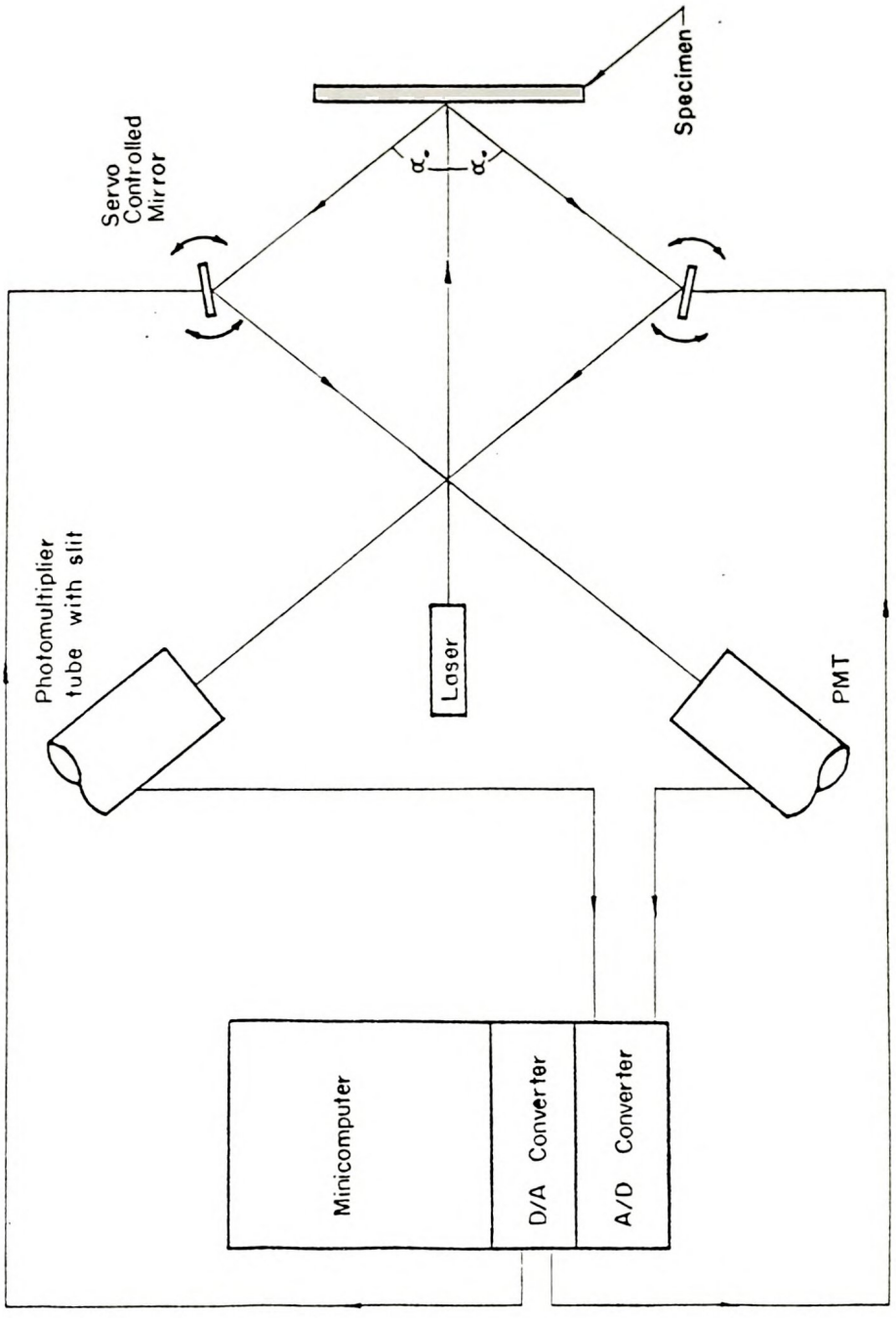

Figure 5 ISG Schematic

swept over the PMT producing an electric analog to the fringe pattern, Figure 6. The mirror position is controlled by the minicomputer and each sweep is broken into 256 consecutively numbered steps at which the corresponding PMT intensity is recorded. For each sweep the minicomputer determines the mirror position numbers associated with the maximum and minimum PMT readings implying bright and dark spots of the fringe pattern. These positions are compared to the positions for the previous sweep to determine fringe movement. Fringe movement is output as the number of mirror positions the first two maximum or minimun locations for a channel have moved and is given a sign depending on whether the shift was toward the laser (+) or away from it (-).

To find the maximum and minimum locations during a sweep the minicomputer compares the sum of the PMT intensities associated with the current mirror position and the last four positions (S_1) to the sum of the intensities of the last five mirror positions (S_2), Figure 7. The sign of (S_1-S_2) indicates the slope of the intensity curve. The sign of (S_1-S_2) for the current mirror position is compared to (S_1-S_2) for the previous position. The slope only changes sign at a maximum or minimum point. If the sign changes from + or 0 to - the mirror position is recorded as a maximum location. If a - or 0 to + shift occurs the mirror position is recorded as a minimum location. The average number of positions between maximum points (called average maximum spacing) is computed by dividing the difference between the first and last maximum location by the total number of maximum locations minus one. The average minimum spacing is computed the same way, Figure 8.

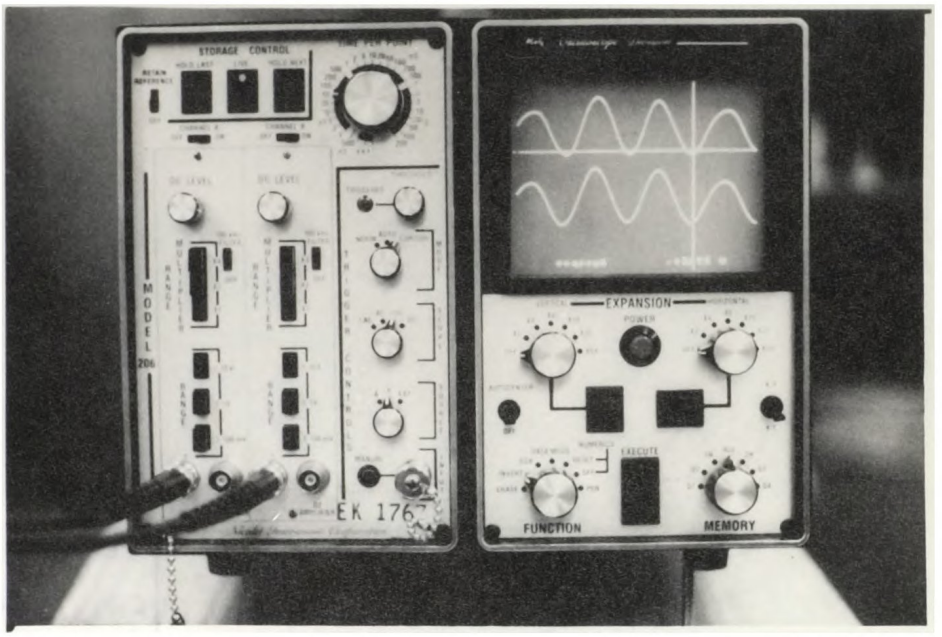

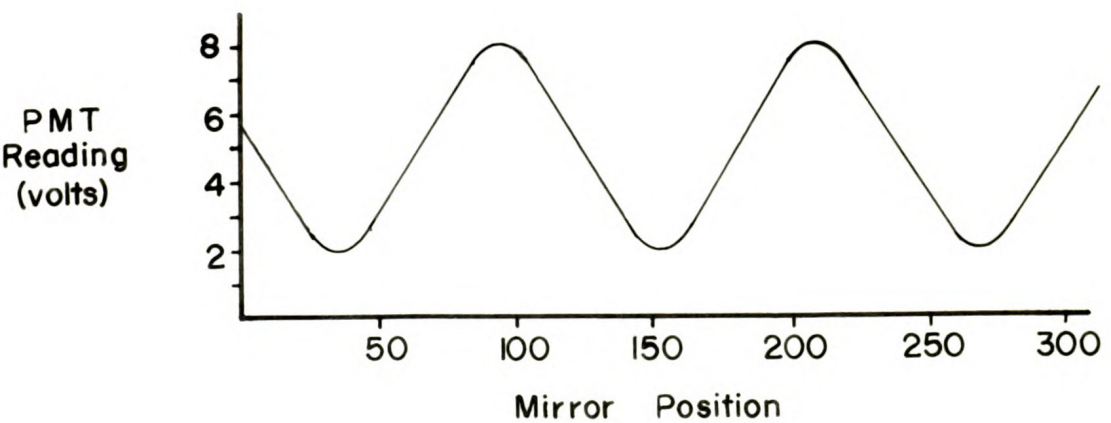

Figure 6 Electric Analog to Fringe Pattern

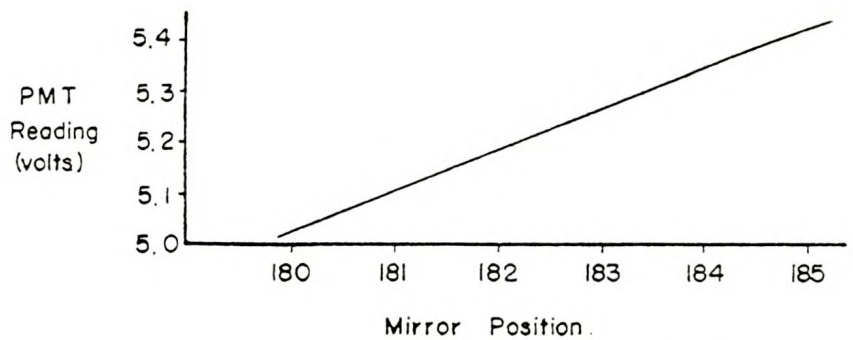

$S_1 = (5.425 + 5.350 + 5.275 + 5.250 + 5.125) = 26.425$

$S_2 = (5.350 + 5.275 + 5.250 + 5.125 + 5.025) = 26.025$

$S_1 - S_2 =$ **Positive** Slope $= 0.400$

Figure 7 S_1 and S_2 for Current Mirror Position 185

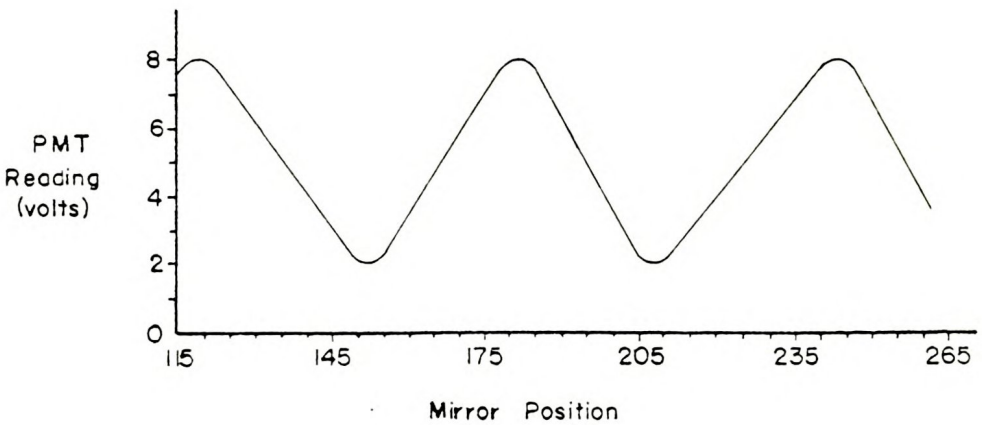

$$\text{Max. Spacing} = \frac{(243 - 119)}{(3 - 1)} = 62$$

$$\text{Min. Spacing} = \frac{(208 - 152)}{(2 - 1)} = 56$$

Figure 8 Determination of Maximum and Minimum Spacing

2.2 Calibration of the I.S.G.

The I.S.G. was calibrated to obtain reliable data without the use of supplementary measuring devices.

The I.S.G. outputs a voltage proportional to the fringe shift. Out put voltage and strain are related by first relating strain to fringe shift then fringe shift to voltage out put.

2.2.1 Strain to Fringe Shift

The equation fundamental to the I.S.G. is:

$$\delta d = \frac{\lambda}{\sin\alpha_o} \delta m \qquad [5]$$

Dividing [5] by the distance between indentations gives:

$$\varepsilon = \frac{\delta d}{d} = \frac{\lambda}{\sin\alpha_o} \frac{\delta m}{d}$$

rearranging this gives:

$$\delta m = \frac{\varepsilon(\sin\alpha_o)}{\lambda} d \qquad [6]$$

where: d = distance between indentations

δd = change in distance between indentations

ε = normal strain between indentations

λ = laser wave length

δ_o = angle between the incident laser and observation point

δ_m = fringe movement in fractions of fringe

2.2.2 Fringe Shift to Voltage

The fringe patterns are swept over photo multiplier tubes (PMT) with mirrors controlled by a minicomputer. Each sweep is broken into 256 consecutively numbered positions at which the PMT voltage is read. The

mimicomputer locates the mirror positions corresponding to maximum and minimum PMT voltage for each sweep and compares them to those for the previous sweep. Also the number of mirror positions between maximum and minimum positions, called fringe spacing (S) is calculated. For each channel the number of positions the first two maximum or two minimum points shift is added (called channel shift total (CST) and equals twice the fringe shift). For rigid body motion the channel patterns shift opposite to each other but shift in the same direction for relative displacement. Therefore, the CST summed over both channels equals four times the relative displacement component of the patterns in terms of mirror positions moved. The CST sum is output as an integer (N). The D/A has 12 bit (i.e. 2^{12} = 4096 increments) converters and a 0-10 volt range. Therefore, one bit of output equals:

$$\frac{10 \text{ Volts}}{4095} = 2.44 \text{ Millivolts}$$

If MV equals the total output in millivolts then

$$MV = N(2.44) \qquad [7]$$

Since N represents four times the shift of the fringe pattern in terms of mirror positions moved dividing N/4 by S gives the shift in terms of fractions of fringes:

$$\delta_m = \frac{N/4}{S} \qquad [8]$$

Rearranging [7] yields:

$$N = \frac{MV}{2.44} \qquad [9]$$

rearranging [8] gives:

$$N = \delta\ m\ (S)4 \qquad [10]$$

equating [9] and [10] leads to:

$$\delta\ m = \frac{MV}{2.44\ (S)4} \qquad [11]$$

2.2.3 Strain to Voltage

Equating [6] and [11] leads to:

$$\frac{\varepsilon\ (\sin \alpha_o)d}{\lambda} = \frac{MV}{2.44\ (S)4} \qquad [12]$$

rearranging gives:

$$MV = \frac{\varepsilon\ (\sin \alpha_o)d}{\lambda}\ 2.44\ (S)4 \qquad [13]$$

where: MV = Millivolts of output

ε = normal strain between indentations

α_o = angle between incident laser and observation point

d = distance (in microns) between indentations

S = average spacing between maximum mirror positions

2.2.4 Calibration Test

A specimen was loaded under strain control. Strain was measured with the I.S.G. and a MTS extensometer (model #632. 13B 20). The strain range was $\pm$ .0048 ε. For this range the extensometer was calibrated at 0.01% error. The I.S.G. was calibrated using Equation [13] with:

$\lambda = 0.6328\mu$

$\alpha = 41.17^o$

$d = 100\mu$

$$\varepsilon = .004$$

$$S = 84$$

Note, S must be determined before you can calibrate. This is easily done by the computer.

Figure 9 shows a plot of I.S.G. strain vs. clip gage strain. Figure 10 shows a sample computer printout listing maximum and minimum locations and spacing.

2.2.5 Resolution

For these tests the average spacing S was 65, $\alpha_o = 43^o$ and $\lambda = 0.6328\mu$. Therefore, the smallest displacement measurable is:

$$\alpha\, d = \frac{1/65}{2} \quad \frac{0.6328}{\sin 43^o} = 0.0071374\mu$$

For the 100 micron gage length used the smallest measurable strain theoretically is: $\frac{0.0071374}{100} = 0.007\%$. However, the actual resolution varies between 0.01% and 0.023% for the test run. This is due to inaccuracy in measuring the exact mirror position for the maximum and minimum locations.

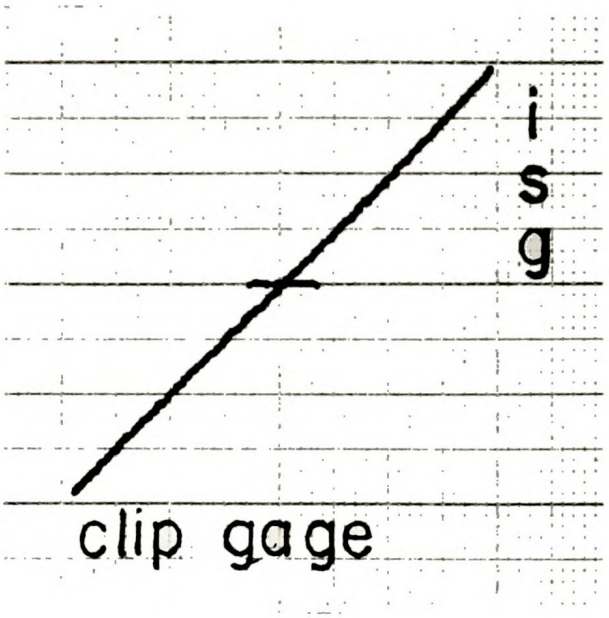

Figure 9 ISG vs. Clip Gage

```
INTERFEROMETRIC STRAIN GAGE COMMANDS:

**     PUSH INT TO JUMP OUT.
**     D-DISPLAY TO OSCILLOSCOPE.
**     P-PRINT MAXIMUM & MINIMUM.
**     R-RUN WITH STRAIN CONTROL.
**     U-USER CONTROL.
**     H-HELP:  PRINT COMMANDS.


D,P,R,U,H?P

CH1   3 MAXS AT:   +ØØ1Ø6 +ØØ172 +ØØ237
      2 MINS AT:   +ØØ138 +ØØ2Ø4

CH2   3 MAXS AT:   +ØØ117 +ØØ182 +ØØ247
      3 MINS AT:   +ØØØ81 +ØØ149 +ØØ215

AVG SEPERATION          WINDOW
 CH1 +ØØØ65             +ØØØ21
 CH2 +ØØØ65             +ØØØ21
```

Figure 10 Computer Print Out of Max and Min

CHAPTER 3

SAMPLES AND MATERIALS

Dimensions for the notched plates and smooth samples are given in Figure 11. Both circular and elliptic notches were examined for each material. Figure 12 shows the specific dimensions for these notches. Figure 13 is a photograph of a smooth sample flanked by notched samples. Figure 14 shows before and after photographs of the indentations for the long life 2024 elliptic sample and the fatigued sample. From Peterson's book (18) K_t was found to be 3.10 for the circular notch and 5.10 for the elliptic notch. However, since the indentations were placed in a finite distance from the notch root (40 microns) the variance in K_t had to be examined. Using the equations developed in Coker's book (19) the variation of K_t was found to be 1.695 percent for the circular notch and 3.202 percent for the elliptical notch. Therefore, K_t equals 3.05 for the circular notch and 4.94 for the elliptic notch. It was thought that longer samples would have to be used to overcome end effects but tests showed uniform stress flow for the sample used. Three materials were tested, 2024 T351 aluminum alloy, 7475 T7351 aluminum alloy and 1018 mild steel. All materials were used as supplied. Table 1 gives material properties.

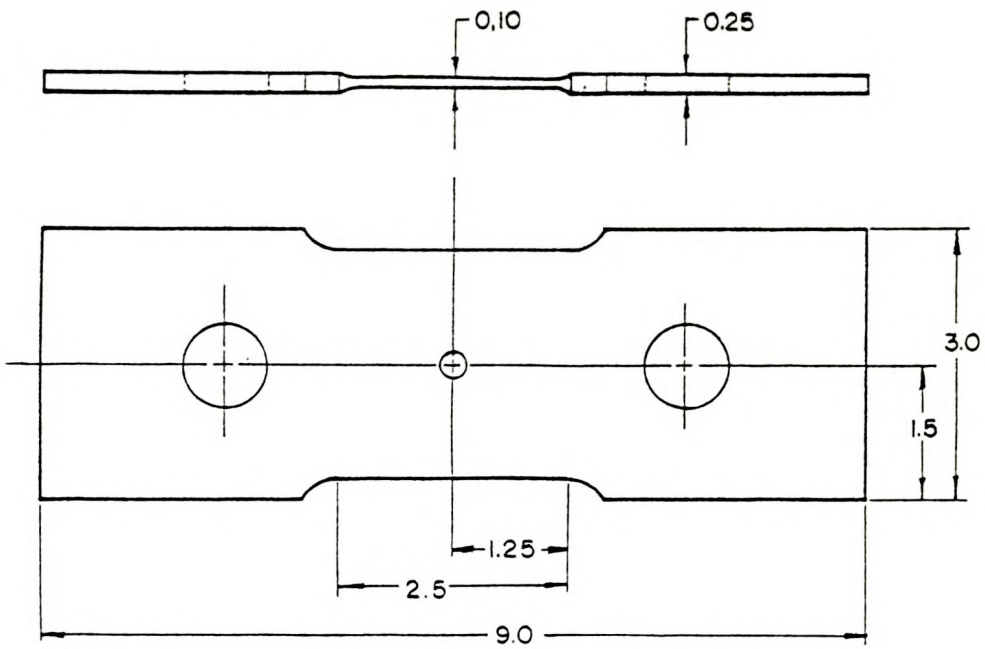

Notched Sample

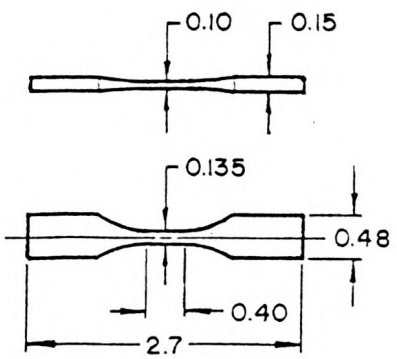

Smooth Sample

Figure 11 Sample Geometry

Ø1.0

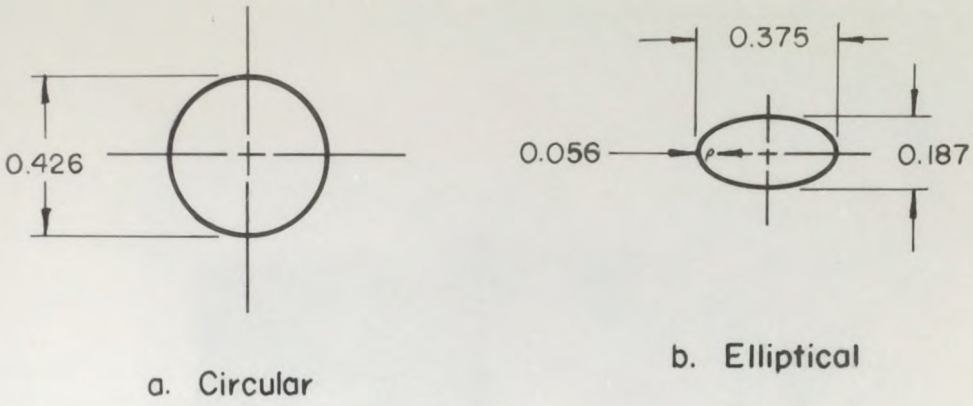

a. Circular

b. Elliptical

Figure 12 Notch Geometry

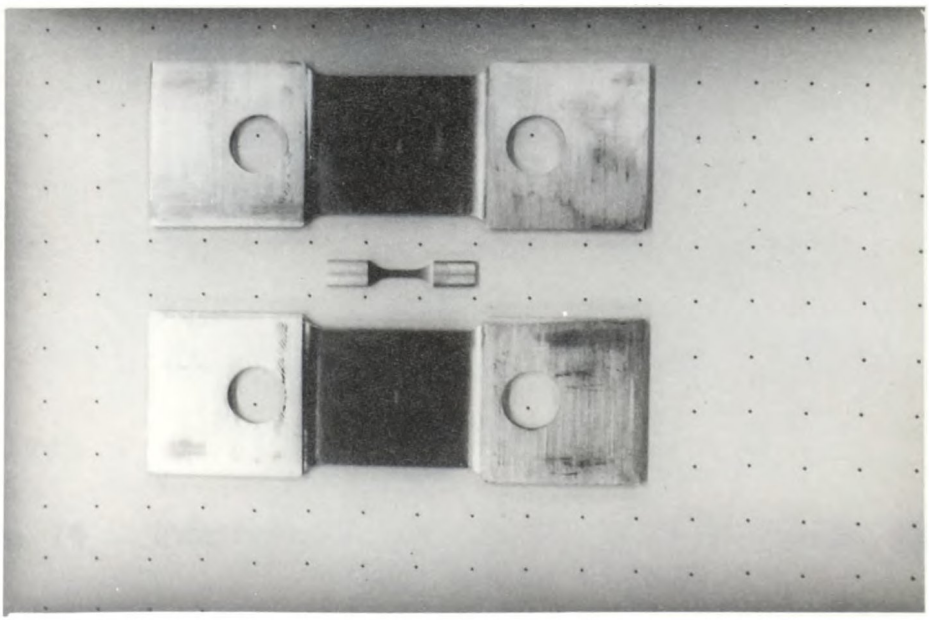

Figure 13 Photograph of Samples

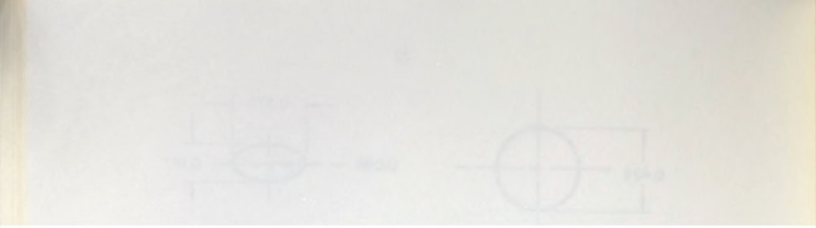

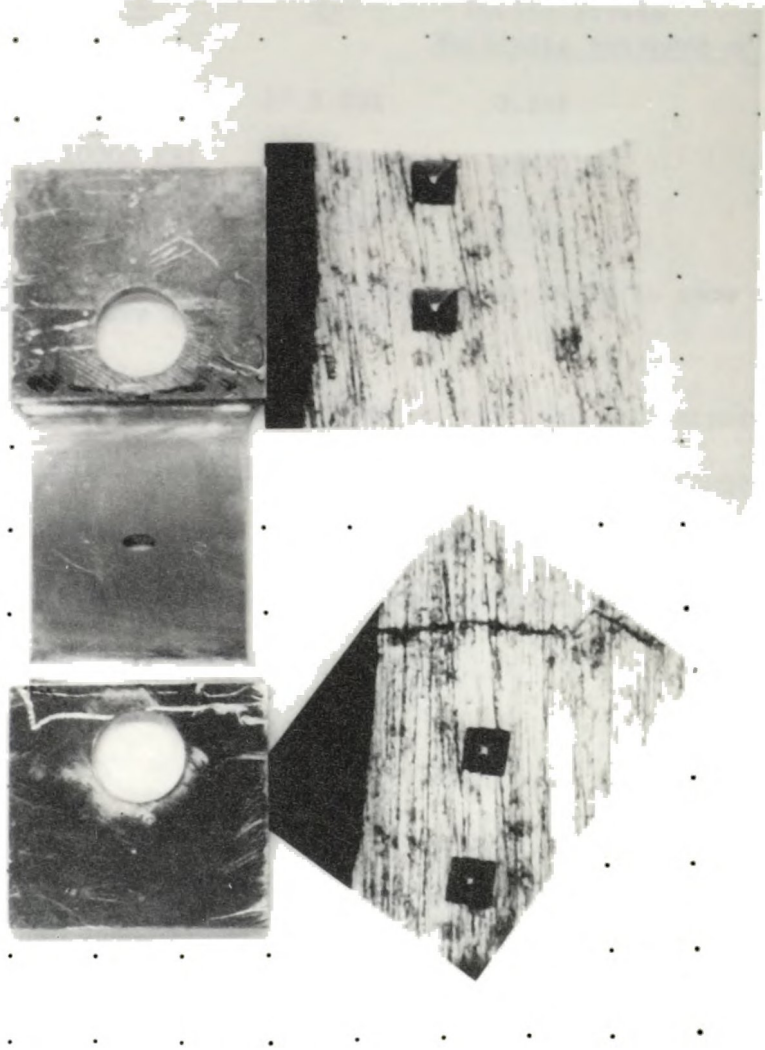

Figure 14 Indentations for 2024 Elliptic Sample Before and After Testing

Table 1. Material Properties

MATERIAL	E	Sy*	Cyclic Strain Hardening exponent n'
1018	30000 KSI	57.8 KSI	0.211
2024 T351	10000 KSI	27.3 KSI	0.075
7475 T7351	10000 KSI	41.1 KSI	0.124

*Actually this is the proportional limit and is given to show that all nominal ranges are indeed elastic.

The 2024 aluminum cyclically hardens at all inelastic strain amplitudes, the 7475 aluminum cyclically softens for all strain ranges tested and the 1018 mild steel softens for strain amplitudes lower than 0.30 percent, hardens for ranges greater than 0.42 percent and is approximately stable at ranges between these values.

CHAPTER 4

EXPERIMENTAL METHODS

All notched tests were run in nominally elastic ranges. The nominal stress (ΔS) is taken as the load divided by the cross-sectional area of the plate if no notch were present. The nominal strain (Δe) is simply:

$$\Delta e = \frac{\Delta S}{E}$$

Where E is Young's Modulus

Local strain ($\Delta \varepsilon$) is measured during testing with the I.S.G. at periodic intervals and plotted as $\Delta \varepsilon$ vs. ΔS. Reproducing this strain in the smooth specimens gives local stresses ($\Delta \sigma$). Inherent in this method is the assumption that shear stresses at the notch root are negligible. Also mean strain is not accounted for as only the ranges were duplicated.

$$K\sigma = \frac{\Delta \sigma}{\Delta S} \qquad K\varepsilon = \frac{\Delta \varepsilon}{\Delta e}$$

$$K_f = (K_\sigma \, K_\varepsilon)^{\frac{1}{2}}$$

All tests were run to failure or a minimum of 1,460,000 cycles. For notched samples failure was determined by the I.S.G. output. If a crack started between the indentations small tensile stresses created large measured strains. Little or no strain is recorded in tension if

the stress between the indentations is relieved by a crack outside the gage length. No output is possible if a crack goes through an indentation. Figure 15 shows output associated with various crack modes. However, some cracks were detected sooner than others. For the smooth samples failure was easily determined by conventional methods. A closed loop servo controlled hydraulic testing machine was used for all tests. Figure 16 shows the test setup. Mounting stresses were reduced with a "woods" metal pot. All tests started in tension and were completely reversed.

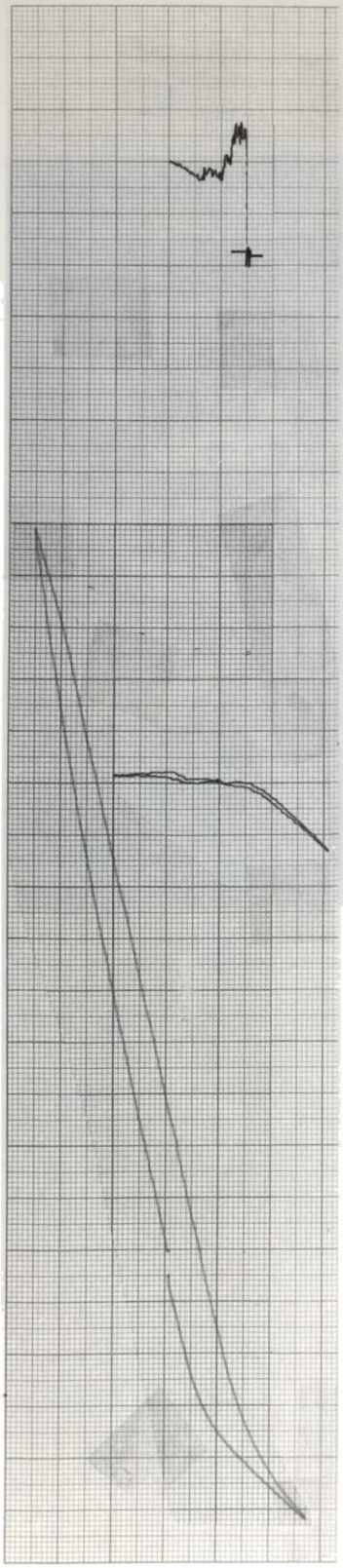

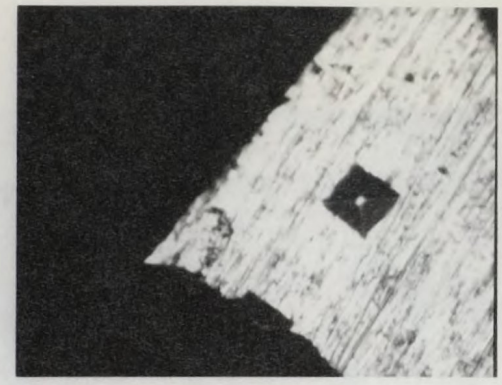

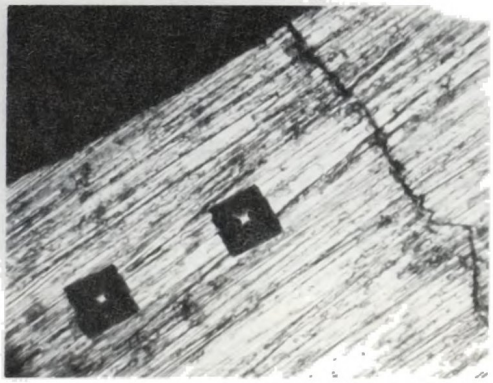

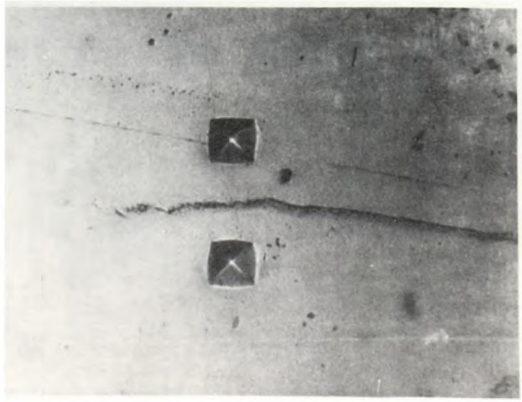

Figure 15 Output for Cracked Samples

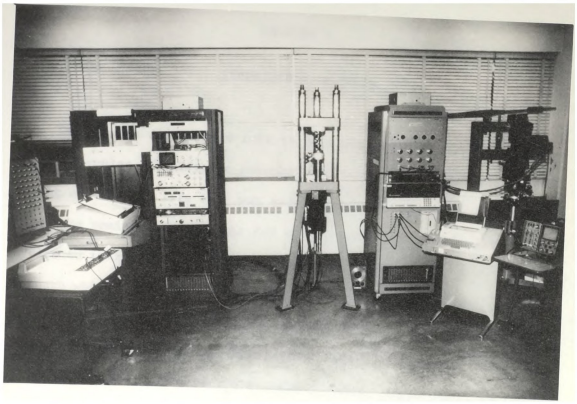

Figure 16 Test Set Up

CHAPTER 5

EXPERIMENTAL RESULTS

The samples are divided into three groups according to material type. Circular and elliptic notches were tested for each material and a long and a short life test was made for each notch geometry. Table 2 gives the nominal stress range for each notched sample, the number of cycles to failure for both the notched and smooth samples and the ranges through which K_σ, K_ε and K_f vary for each test. These ranges do not reflect trends during life (other than scatter) but are helpful when comparing trends due to materials, life and notch geometry. Figures 17 through 22 are plots of K_σ, K_ε, and K_f versus life. Each plot shows a long and short life test for a given material and notch geometry. Scales for these plots were chosen to best show the distribution for each set of tests. Figures 23 through 28 are duplicates of Figures 17 through 22 showing only K_f and are all drawn to the same scale to facilitate comparisons between the test sets.

Table 2. Test Data

		N_f		Range Over Test			
Sample	$\Delta S/2$	Notched	Smooth	K_ε	K_σ	K_f	Over All
1018	KSI						
Ellipse	27.5	5300	5245	4.00→5.32 1.32	1.62→2.53 0.914	2.75→3.28 0.53	1.62→5.32 3.7
Ellipse	7.0	3,243,010*	2,179,435*	3.50→3.96 0.46	3.40→3.88 0.48	3.55→3.92 0.37	3.40→3.96 0.56
Circle	15.2	824,780	105,484	2.95→3.22 0.27	2.40→2.97 0.57	2.65→2.99 0.34	2.4 →3.22 0.82
Circle	28.0	20,000	16,843	2.71→3.25 0.54	1.52→2.26 0.73	2.21→2.5 0.29	1.5 →3.25 1.75
2024							
Ellipse	8.0	700,000	101,480	4.67→5.05 0.38	3.89→4.09 0.20	4.22→4.55 0.325	3.89→5.05 1.16
Ellipse	24.0	300	254	3.87→4.34 0.47	3.20→3.76 0.56	3.53→4.04 0.51	3.20→4.34 1.14
Circle	12.0	103,893	85,509	2.61→2.92 0.31	2.81→3.06 0.25	2.71→3.02 0.31	2.61→3.06 0.45
Circle	20.0	20,000	4,295	2.53→2.99 0.46	2.48→2.68 0.20	2.58→2.84 0.26	2.47→2.99 0.52
7475							
Ellipse	12.0	22,277	16,311	3.50→3.59 0.09	3.44→3.57 0.13	3.45→3.58 0.13	3.44→3.59 0.15
Ellipse	7.0	2,244,603	98,148	3.66→3.96 0.30	3.70→4.05 0.35	3.71→4.00 0.29	3.66→4.05 0.39
Circle	27.0	600	756	2.72→3.39 0.67	2.03→2.13 0.10	2.35→2.68 0.33	2.03→3.39 1.36
Circle	11.6	1,460,000*	82,902	2.69→2.80 0.11	2.56→2.72 0.16	2.62→2.75 0.13	2.62→2.80 0.18

*Did not break and was pulled from test at cycle given.

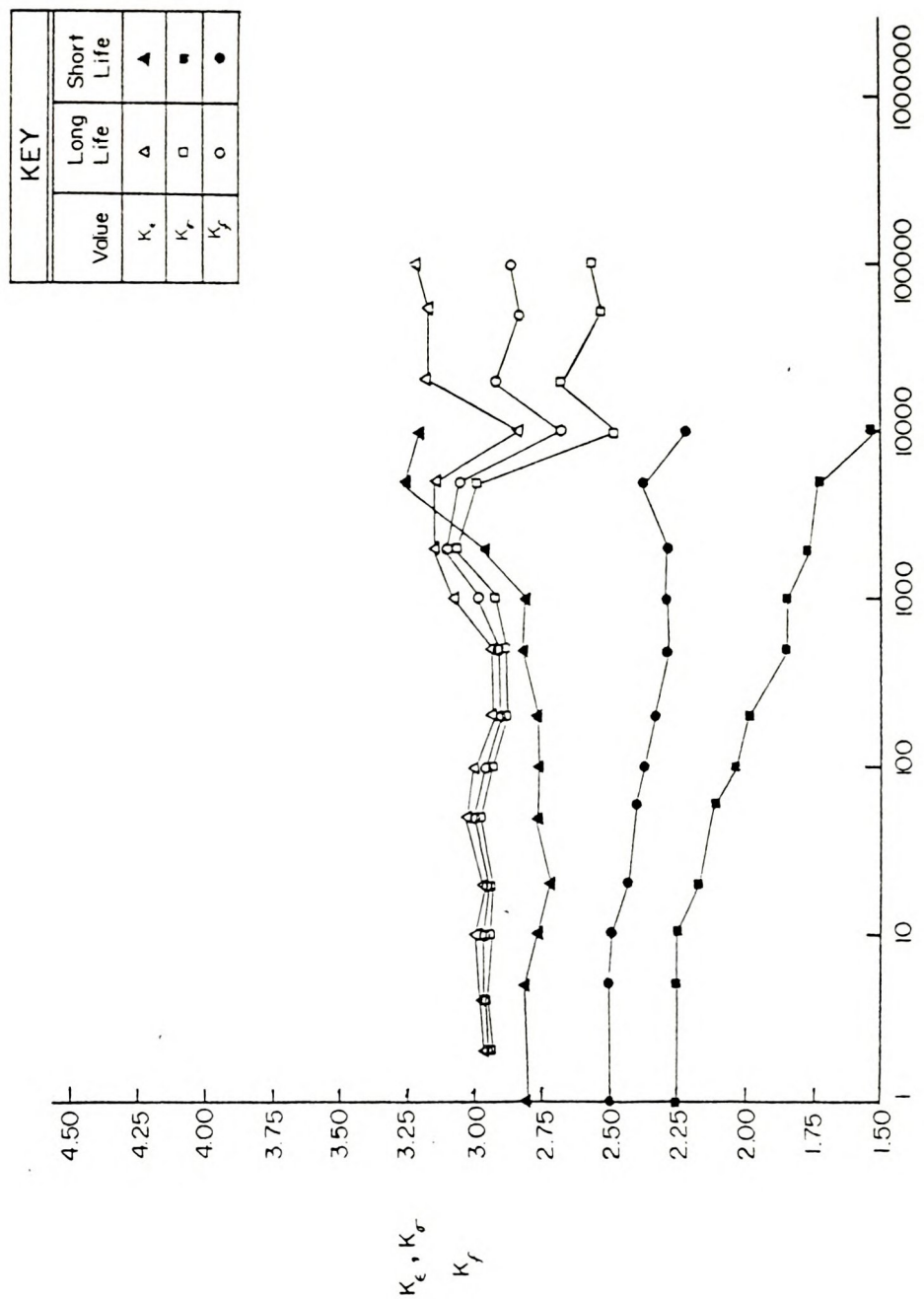

Figure 17 K_ϵ, K_σ, and K_f vs. Life for 1018 Mild Steel — Circular Notches

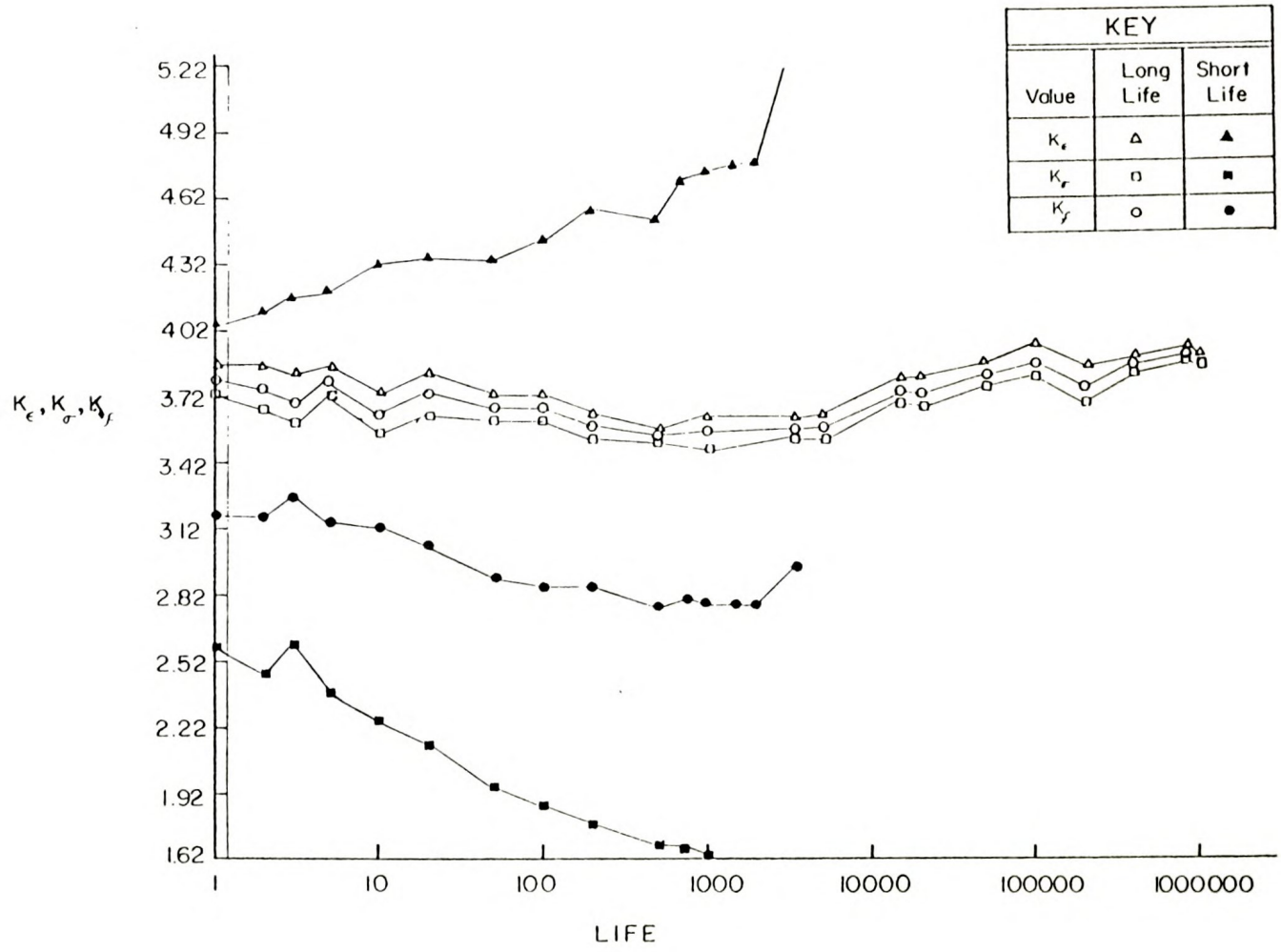

Figure 18 K_ϵ, K_σ, and K_f vs. Life for 1018 Mild Steel — Elliptical Notches.

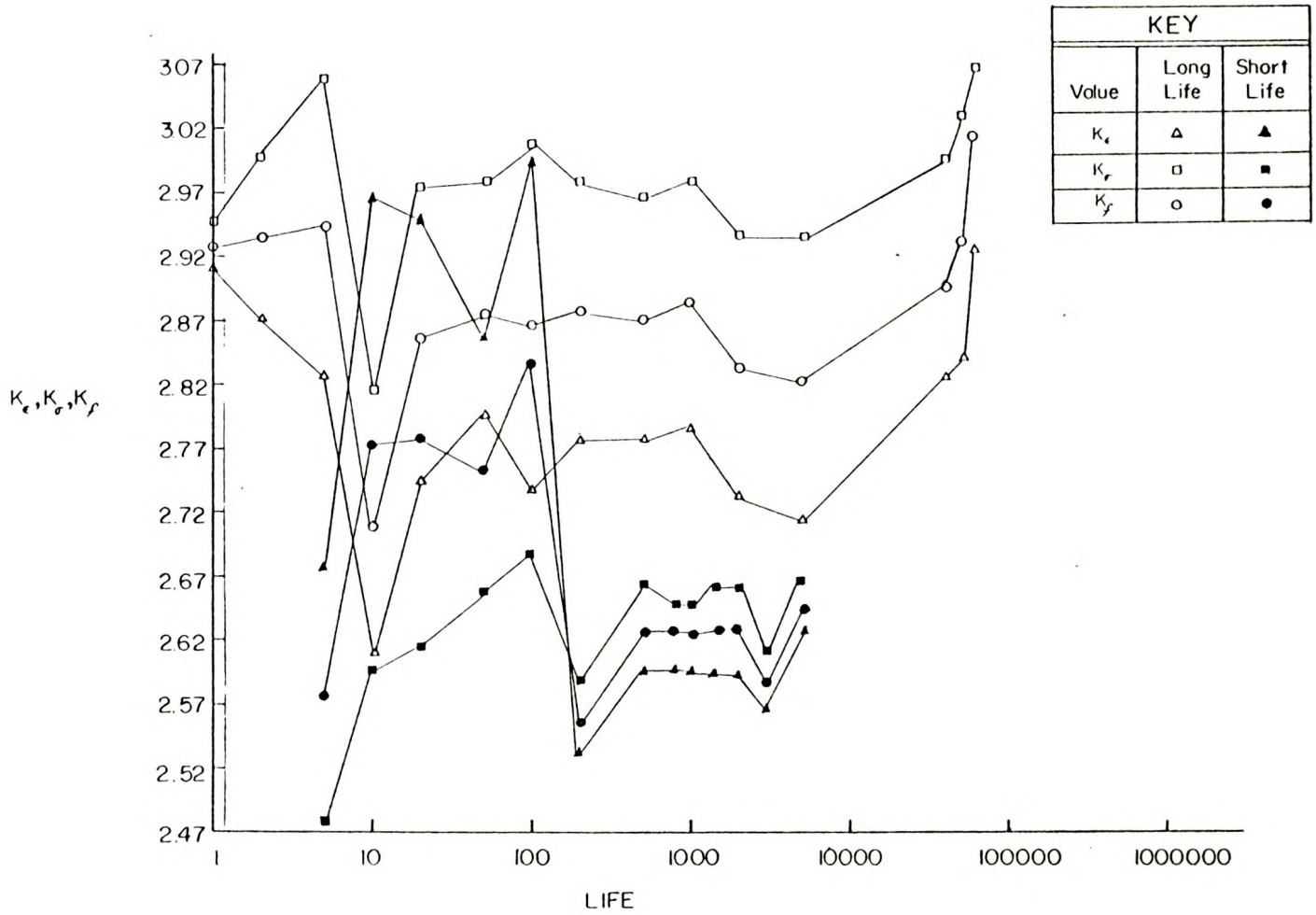

Figure 19 K_ϵ, K_σ and K_f vs. Life for 2024 Aluminum — Circular Notches

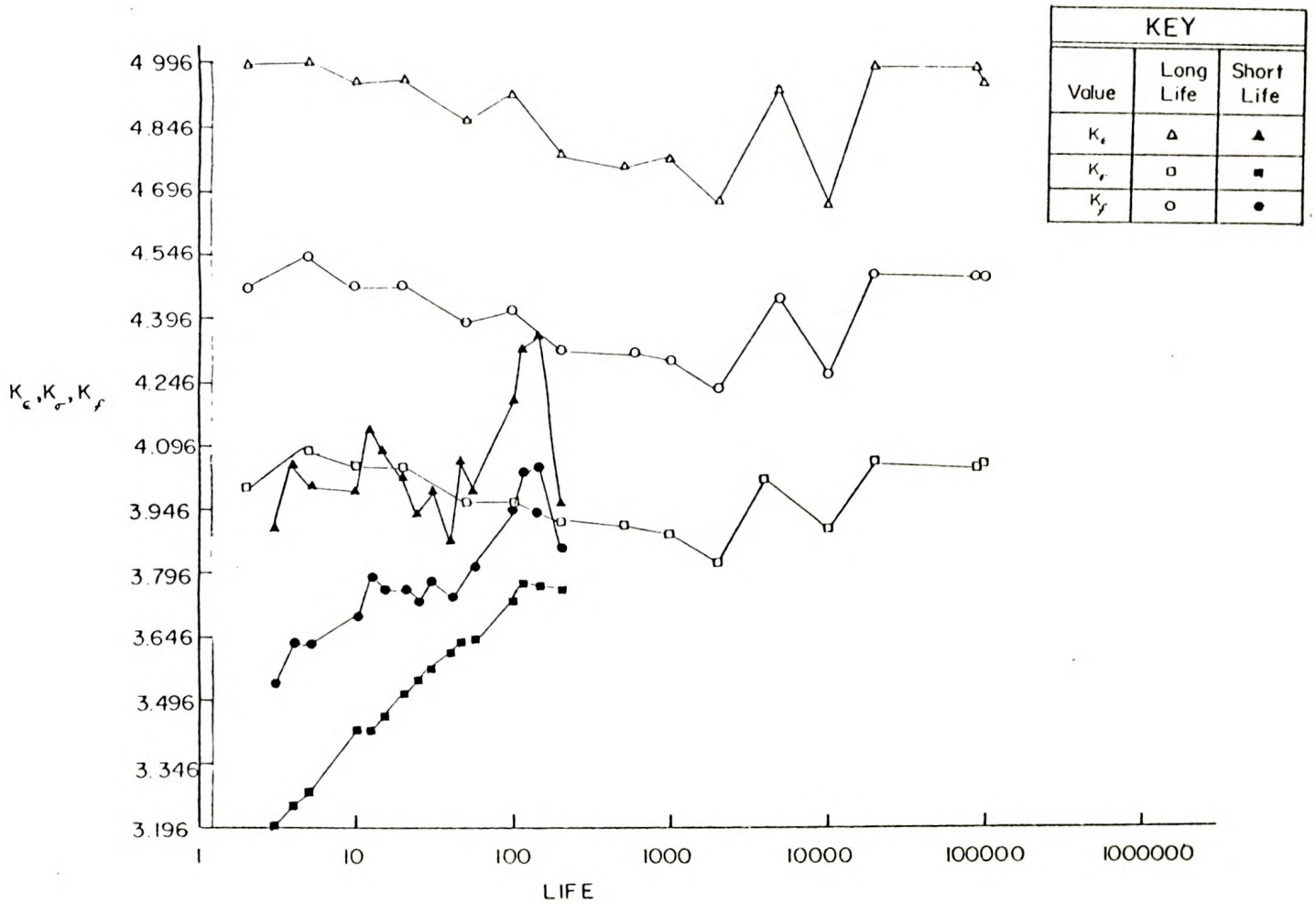

Figure 20 K_ϵ, K_σ and K_f vs. Life for 2024 Aluminum — Elliptical Notches

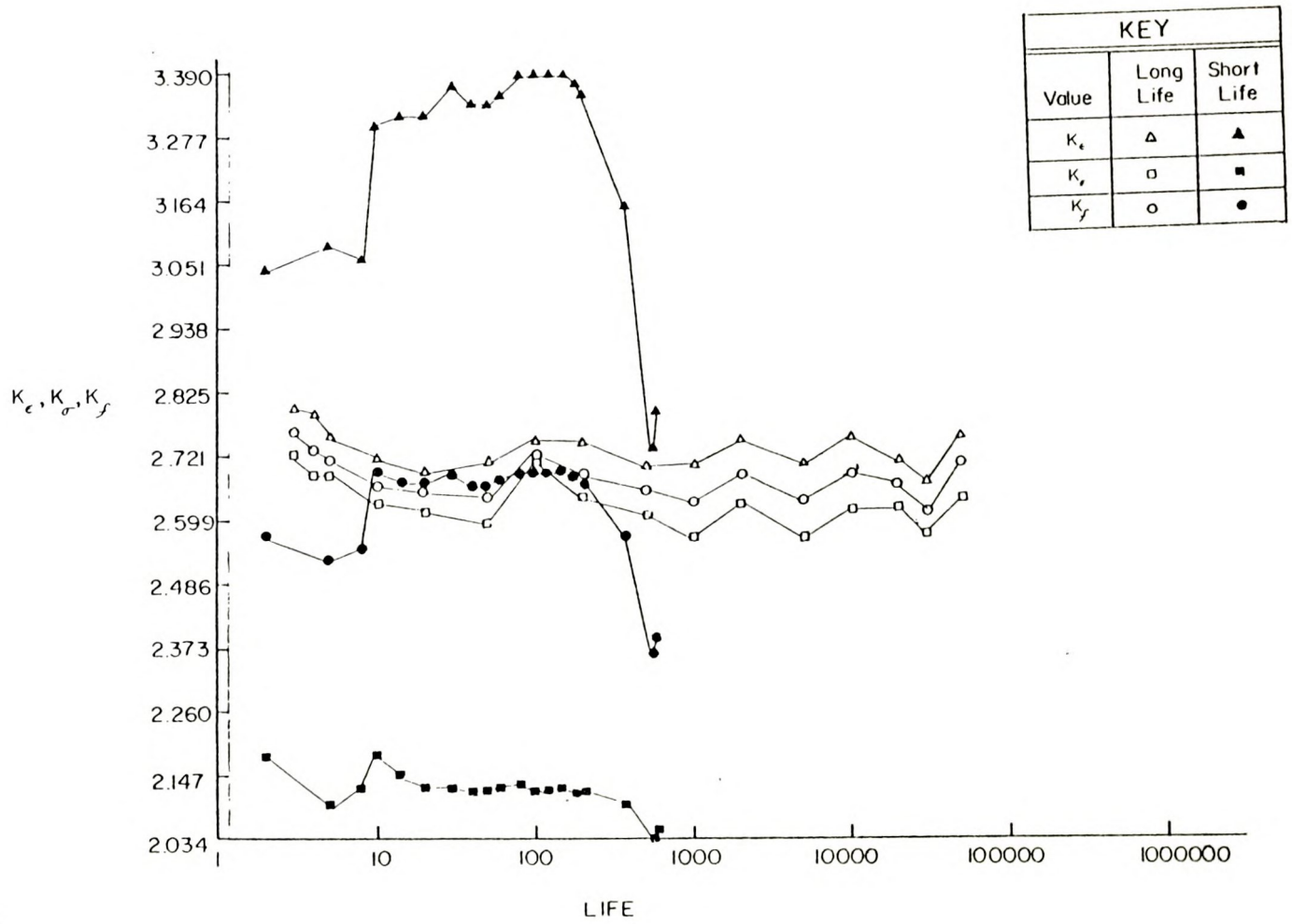

Figure 21 K_ϵ, K_σ and K_f vs. Life for 7475 Aluminum — Circular Notches

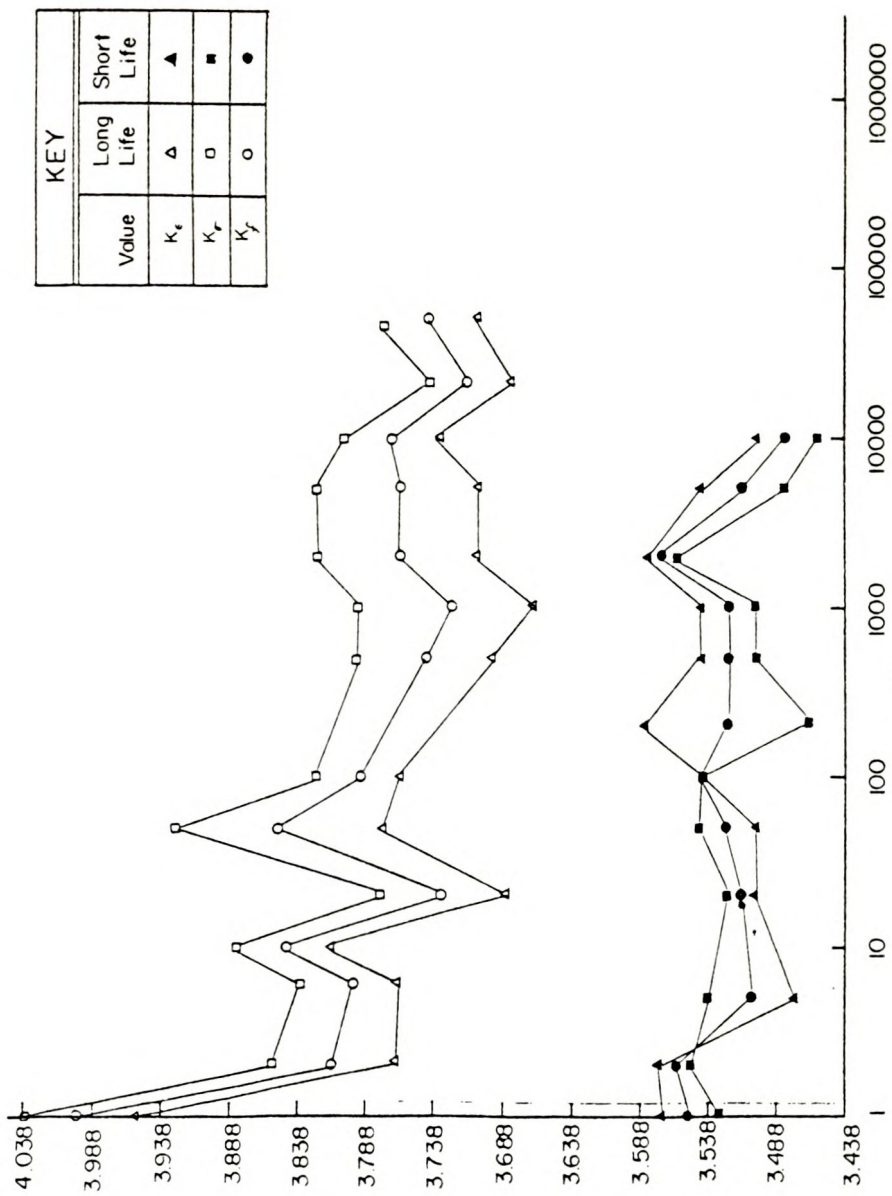

Figure 22 K_ϵ, K_σ and K_f vs. Life for 7475 Aluminum — Elliptical Notches

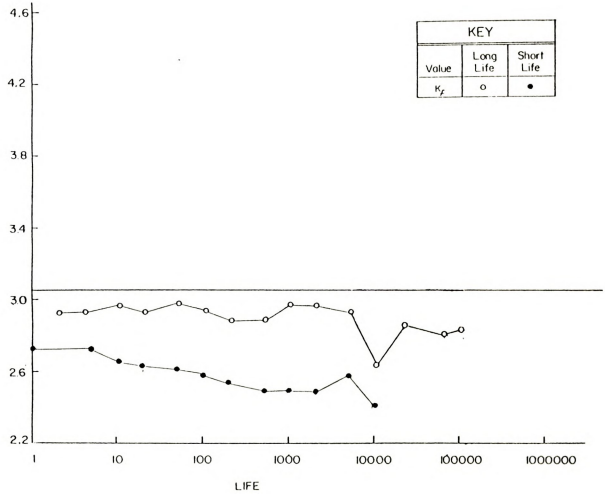

Figure 23 K_f vs. Life for 1018 Mild Steel – Circular Notches

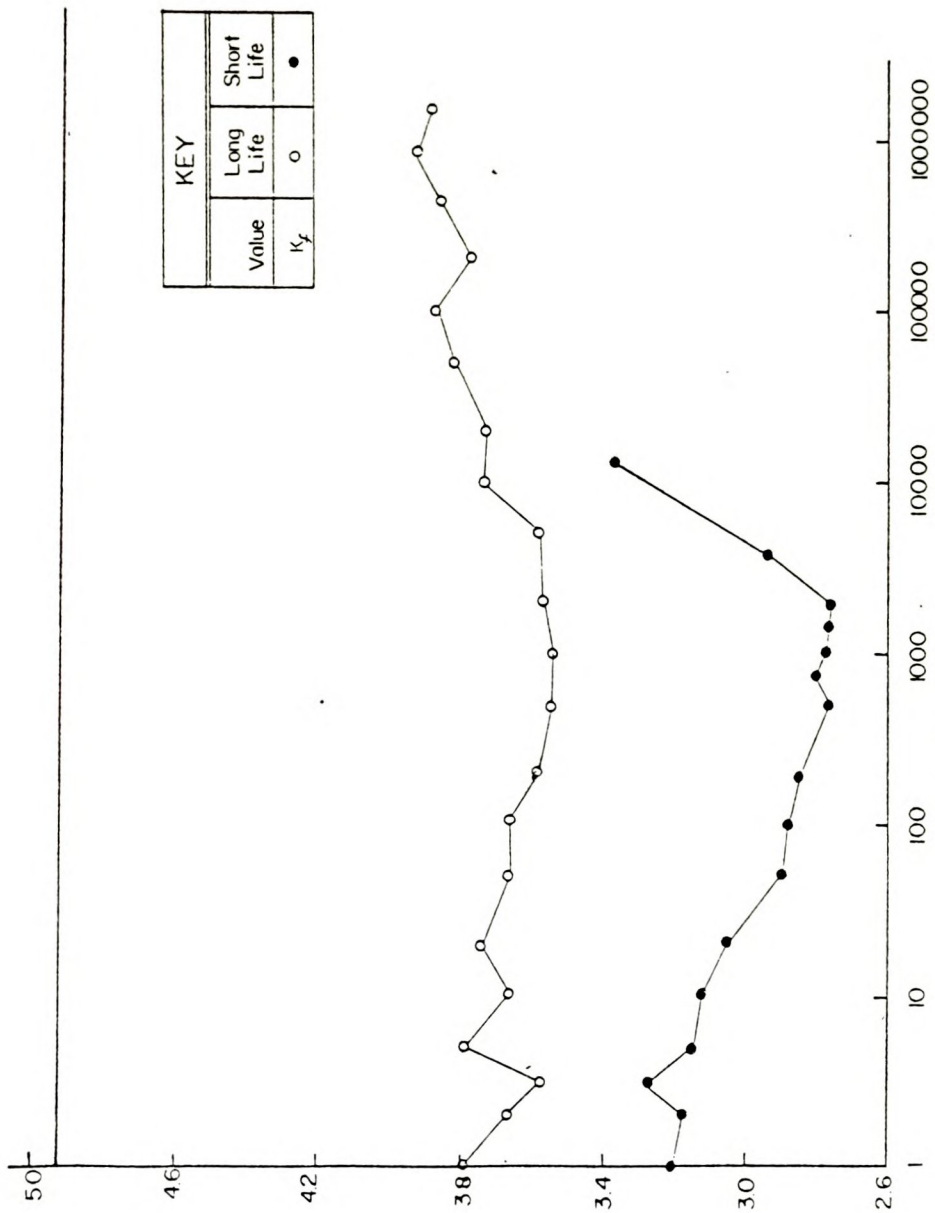

Figure 24 K_f vs. Life for 1018 Mild Steel— Elliptical Notches

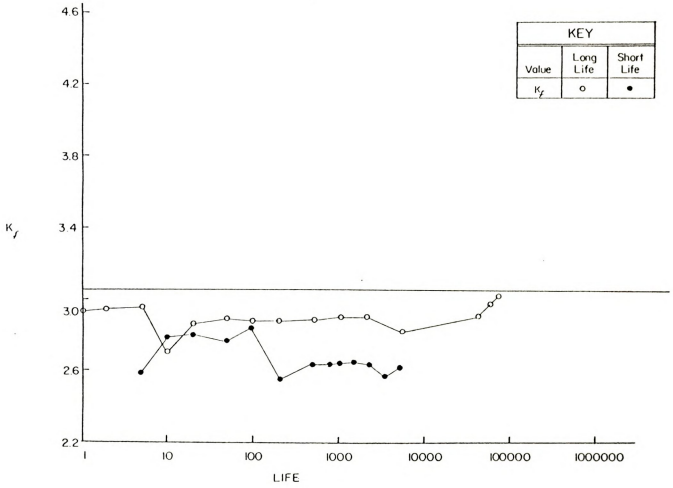

Figure 25 K_f vs. Life for 2024 Aluminum — Circular Notches

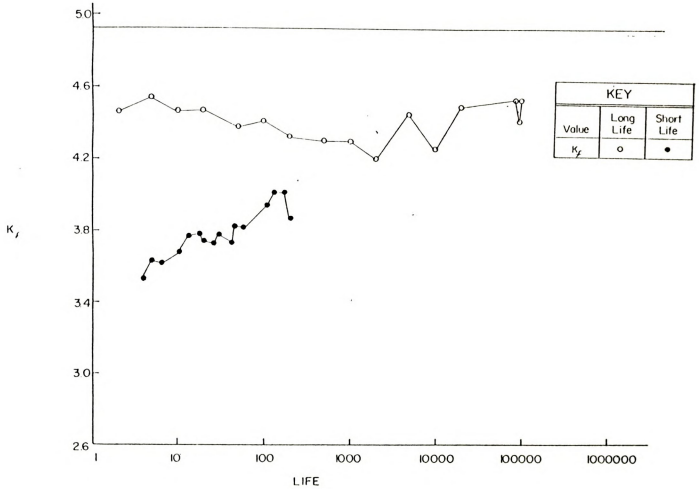

Figure 26 K_f vs. Life for 2024 Aluminum — Elliptical Notches

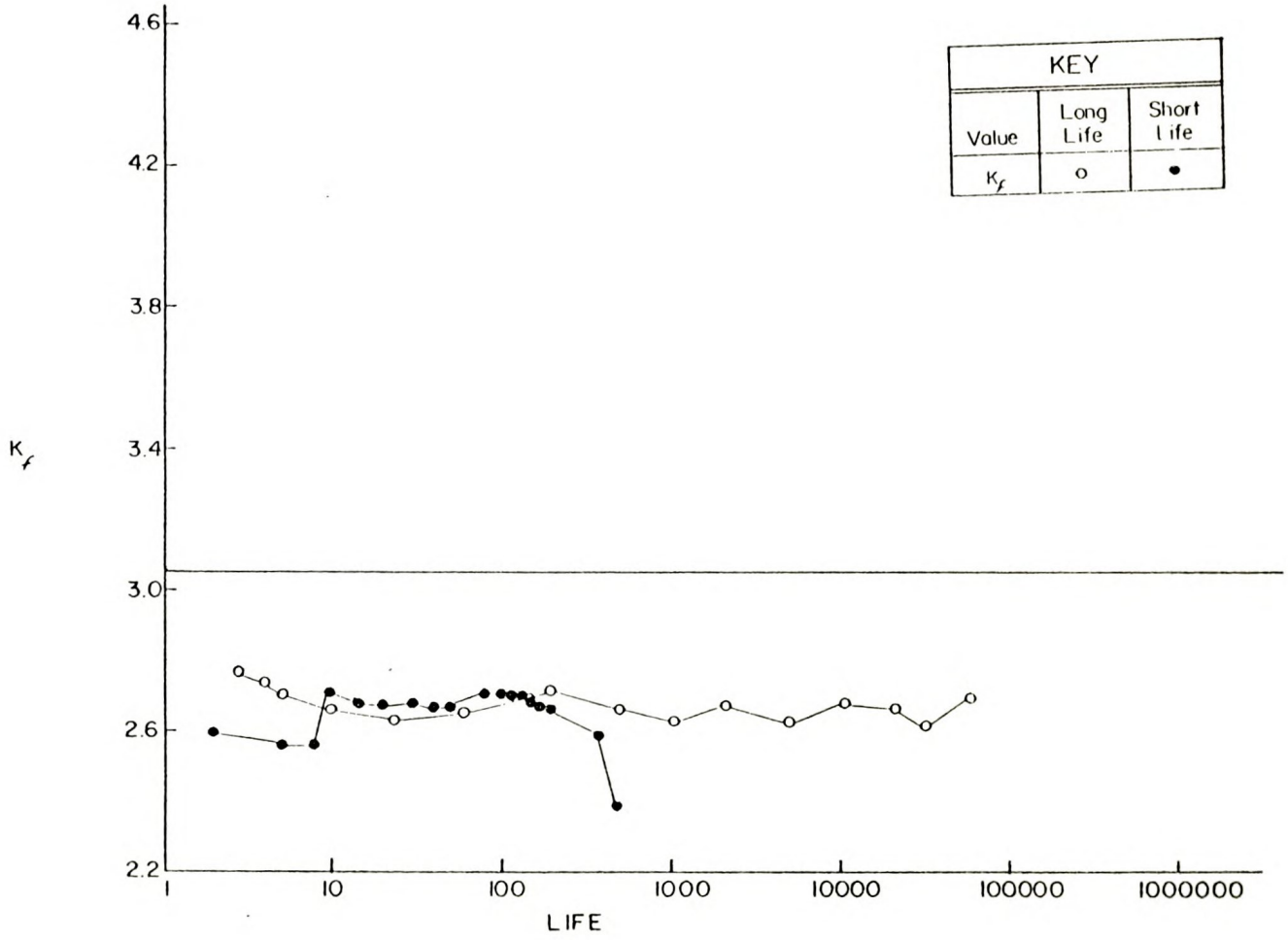

Figure 27 K_f vs. Life for 7475 Aluminum — Circular Notches

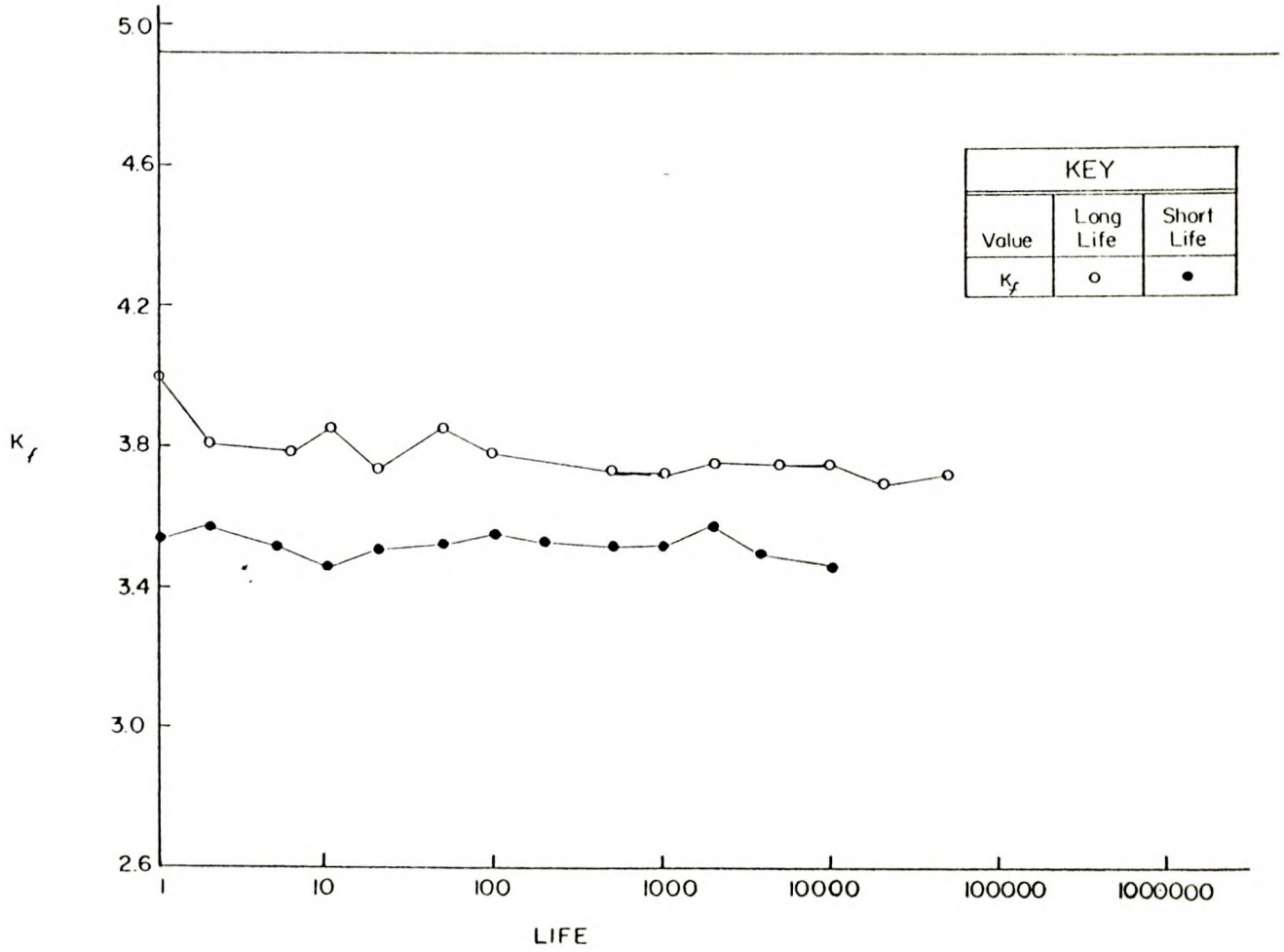

Figure 28. K_f vs. Life for 7475 Aluminum — Elliptical Notches

CHAPTER 6

SUMMARY AND CONCULSIONS

For all tests K_f was less than K_t and for all materials the variance was greater for the elliptic notches than for the circular notches. For 2024 aluminum the greatest difference between K_t and K_f in terms of percent of K_t for elliptic versus circular notches was 8 percent versus 5 percent; for 7475 aluminum, 23 percent versus 11 percent and 23 percent versus 7 percent for 1018 mild steel. Note the K_f values for the 2024 samples were closest to K_t for both notch geometries and for 7475 the farthest from K_t for all materials tested.

Table 2 shows excellent correlation between fatigue life of the smooth and notched samples. In all cases but one N_f for the smooth sample was less than N_f for the corresponding notched sample. This is just as expected because notched samples were run until the I.S.G. output was effected by a crack and that happens only after the crack extends through the indentation site. This strongly suggests that notch root strain can be modeled with smooth samples in which only the normal notch root strain is reproduced.

The variance of K_σ, K_ε, and K_f depends on the material and the 1018 mild steel and 2024 aluminum show variances with strain range. For 1018 mild steel long life circular and elliptical tests K_ε, K_σ, and K_f are stable throughout life. During short life cycling K_σ decreases while

K_ε increases and K_f tends to decrease with life. For both notch types K_f is lower for short life.

K_f for low cycle 2024 aluminum samples approaches stable long life values. This is best seen in the elliptic samples (Figure 18). A large jump in K_f, K_σ, and K_ε occurs at cycle 200 for the short life circular sample. This transition is suspect because the local hystersis loops radically change shape for the smooth sample but do not for the notched sample between cycle 100 and cycle 200 and N_f for the smooth sample is much less than N_f for the notched sample. It is possible that while reproducing the notch strains in the smooth sample a system malfunction caused an overload. Due to lack of samples another smooth sample was not run. It is interesting to note that for the entire long life circular test K_σ was greater than K_ε. All values do not stabilize for the 2024 circular samples until after twenty cycles whereas the elliptic long life values are stable throughout the entire life. The elliptic short life values never stabilize but shift smoothly toward the stable long life values with life.

K_f, K_σ, and K_ε for 7475 aluminum stabilize after the first ten cycles for the circular samples and after the first twenty cycles for the elliptic. K_ε is less than K_σ throughout the entire long life elliptic test and for portions of the short life test. For both sets of tests stable values of K_f for short life are equal to or near stable long life values of K_f.

In general the elliptical samples exhibit stable (or for 2024 low life, consistent) notch concentration factors throughout life while the circular samples (with the exception of 1018 mild steel) required ten to twenty cycles to stabilize or develop smooth trends. It must be

noted that the 2024 elliptic low life sample never stabilized even though $N_f = 254$. For both aluminums strain range had little or no effect on stable K_f values for circular samples, however, for elliptical samples 7475 showed two close but distinct values for long and short life while short life 2024 tended toward stable long life values of K_f. The 1018 mild steel reacted consistently for both notch types with a lower diminishing K_f for short life and smooth stable trends throughout life for all strain ranges.

To summarize: The problems associated with mounted strain gages have been overcome with the I.S.G. and the techniques of reproducing notch strain in smooth samples is a good one for obtaining notch stresses. The characteristics of cyclic K_f seem to be material dependent. For 1018 mild steel K_f is stable throughout life with no initial stabilization period and decreases with increasing strain range. Also for larger strain ranges K_f decreases with life. For 2024 and 7475 aluminum circular notches K_f stabilizes after twenty cycles to a given value for each material reguardless of strain range. For elliptic samples 2024 short life K_f values tend toward stable long life values which 7475 exhibits decreasing values for K_f with increasing life. In general, for any material elliptic samples stabilized quicker but showed greater variance from K_t than circular samples.

There is still much to learn in this area. These tests should be extended to shorter life regions and comprehensive life-K_f trends developed and modeled for various materials. Presently work is being done in these areas.

LIST OF REFERENCES

LIST OF REFERENCES

1. Neuber, H., "Theory of Stress Concentration for Shear Strained Prismatic Bodies with Arbitrary Non-linear Stress and Strain Law," Journal of Applied Mechanics, Vol. 28, No. 4, Dec. 1961, pp. 544-550.

2. Gowda, C. U. B., and T. H. Topper, "On the Relation Between Stress and Strain Concentration Factors in Notched Members in Plane Stress," Journal of Applied Mechanics, Vol. 37, No. 1, Mar. 1970, pp. 77-84.

3. Topper, T. H., R. M. Wetsel, and JoDean Morrow, "Neuber's Rule Applied to Fatigue of Notched Specimens," Journal of Materials JMLSA, Vol. 4, No. 1, Mar. 1969, pp. 200-209.

4. Crews, J. H., Jr., and H. F. Hardrath, "A Study of Cyclic Plastic Stresses at a Notch Root," Experimental Mechanics, Vol. 6, No. 6, June 1966, pp. 313-320.

5. Box, W. A., "The Effect of Plastic Strains on Stress Concentration," Proceedings, Society for Experimental Stress Analysis, Vol. 8, No. 21, 1951, pp. 99-110.

6. Griffith, G. E., "Experimental Investigation of the Effect of Plastic Flow in a Tension Paper with a Circular Mole," NACA Technical Note 1705, 1949, National Advisory Committee for Aeronautics.

7. Blatherwick, A. A. and B. K. Olsen, "Stress Redistribution in Notched Specimens Under Cyclic Stress," ASD Technical Report 61-451, 1961, Aeronautical Systems Division, Wright-Patterson Air Force Base, Dayton, Ohio.

8. Gowda, C. V. D. and T. H. Topper, "Cyclic Deformation Behavior of Notched Mild Steel Plates in Plane Stress," Experimental Mechanics, Vol. 12, No. 8, Aug. 1972, pp. 359-367.

9. Leis, B. H., "Cyclic Inelastic Deformation Behavior of Thin Notched Plates," M.A.Sc. Thesis, University of Waterloo, Canada, 1972.

10. Evans, R. J. and K. S. Pister, "Constitutive Equations for a Class of Nonlinear Solids," International Journal of Solids and Structures, Vol. 2, 1966, pp. 427-445.

11. Wetzel, R. M., "Smooth Specimen Simulation of the Fatigue Behavior of Notches," Journal of Materials, JMLSA, Vol. 3, No. 3, Sept. 1968, pp. 646-657.

12. Morrow, JoDean, "Cyclic Plastic Strain Energy and Fatigue of Metals," Internal Friction, Damping and Cyclic Plasticity, ASTM STP 378, American Society for Testing and Materials, Philadelphia, 1965, pp. 45-87.

13. Manson, S. S. and M. H. Hirschberg, "Crack Initiation and Propagation in Notched Fatigue Specimens," Proceedings of the First International Conference on Fracture, Vol. 1, Japanese Society for Strength and Fracture of Materials, 1966, pp. 479-498.

14. Peterson, R. E., "Fatigue of Metals in Engineering and Design," Thirth-Sixth Edgar Marburg Lecture, American Society for Testing and Material, 1962; Materials Research and Standards, Vol. 3, No. 2, Feb. 1963, pp. 122-139.

15. Dolan, T. J., "Non-linear Response Under Cyclic Loading Conditions," Proceedings of the 9th Midwest Mechanics Conference, Aug. 1965, pp. 3-21.

16. Peterson, R. E., "Notch-Sensitivity," Metal Fatigue, Sines and Waisman, eds., McGraw-Hill, New York, 1959, pp. 293-306.

17. Leis, B. N., C. V. B. Gowda, and T. H. Topper, "Some Studies of the Influence of Localized and Gross Plasticity on the Monotonic and Cyclic Concentration Factors," Journal of Testing and Evaluation, JTEVA, Vol. 1, No. 4, July 1973, pp. 341-348.

18. Peterson, R. E., "Stress Concentration Factors," John Wiley and Sons, Inc., 1974, pp. 150-196.

19. Coker, E. G., and L. N. G. Filon, "A Treatise on Photoelasticity," 2nd Ed., Cambridge University Press, 1957.

20. Sharpe, W. N., Jr., "The Interferometric Strain Gage," Experimental Mechanics 8, April 1968, pp. 164-170.

21. Sharpe, W. N., Jr., "Interferometric Surface Strain Measurement," International Journal of Non-Destructive Testing 3, 1971, pp. 51-76.

22. Sharpe, W. N., Jr., "A Short Gage-Length Optical Gage for Small Strain," Experimental Mechanics, 14, 1974, pp. 373-377.

23. Sharpe, W. N., Jr., "Development and Application of an Interferometric System for MEasuring Crack Displacements," Final Report on Grant NSG 1148, June 1976.

MICHIGAN STATE UNIVERSITY LIBRARIES
3 1293 03196 0119